

# Transformable Linkage-Based Gripper for Multi-Mode Grasping and Manipulation

Junghan Kwon<sup>1\*</sup>, David Bombara<sup>2\*</sup>, Clark Teeple<sup>2</sup>, Joonhaeng Lee<sup>3</sup>, Chuck Hoberman<sup>3</sup>, Robert Wood<sup>2</sup>, and Justin Werfel<sup>2</sup>

**Abstract**—Gripper hardware design often involves a trade-off between distinct and sometimes opposing goals (e.g., high grasping force vs. gentleness). To address this trade-off within a single device, we present a *multi-mode* gripper with fingers that are scissor linkages, that can actively transform between three distinct modes by varying the number and locations of mechanical singularities. Each of these modes has properties that are suitable for specific needs. MODE 1 provides high grip strength, using a short lever arm and rigid structure. MODE 2 allows precise finger positioning and in-hand manipulation, using two independently controlled DOFs per finger. MODE 3 provides underactuated grasping that can passively adapt to delicate or irregularly shaped objects, with four DOFs per finger. The kinematic relationships, joint torques, and fingertip forces are derived analytically for each of the three modes. Gripper performance and the kinematic model are verified experimentally.

**Index Terms**—Grippers and Other End-Effectors; Actuation and Joint Mechanisms; Tendon/Wire Mechanism

## I. INTRODUCTION

Manipulation tasks in robotics are critical to a wide range of applications, including manufacturing, assembly, packaging, material handling, and search and rescue operations which involve grasping, orienting, assembling, or crushing objects [1]. Some applications require high grip force to securely grasp a heavy object, whereas other applications focus on precision and dexterity to achieve a goal [2]. Therefore, the designer of a gripper should carefully determine its kinematics, dimensions, and geometries according to the weight, size, shape, and mechanical properties of the objects it is intended

Manuscript received: June 13, 2023; Revised September 9, 2023; Accepted October 8, 2023.

This paper was recommended for publication by Editor Hong Liu upon evaluation of the Associate Editor and Reviewers' comments (*Corresponding author: David Bombara*).

This work was supported by a Space Technology Research Institutes grant (number 80NSSC19K1076) from NASA's Space Technology Research Grants Program, the National Science Foundation Graduate Research Fellowship Program, and the National Research Foundation of Korea (NRF) funded by the Ministry of Education (2021R1A6A3A14044384).

<sup>1</sup>Junghan Kwon is with the School of Mechanical Engineering, Pusan National University, Busan, Korea (email: jhkwon85@pusan.ac.kr).

<sup>2</sup>David Bombara, Clark Teeple, Robert Wood, and Justin Werfel are with the John A. Paulson School of Engineering and Applied Sciences, Harvard University, Boston, MA 02134, USA (email: davidbombara@g.harvard.edu, cbteeple@g.harvard.edu, rjwood@seas.harvard.edu, jkwerfel@seas.harvard.edu).

<sup>3</sup>Joonhaeng Lee and Chuck Hoberman are with the Graduate School of Design, Harvard University, Cambridge, MA 02138 (email: joonhaenglee@gsd.harvard.edu, choberman@gsd.harvard.edu).

\*Authors contributed equally

Digital Object Identifier (DOI): see top of this page.

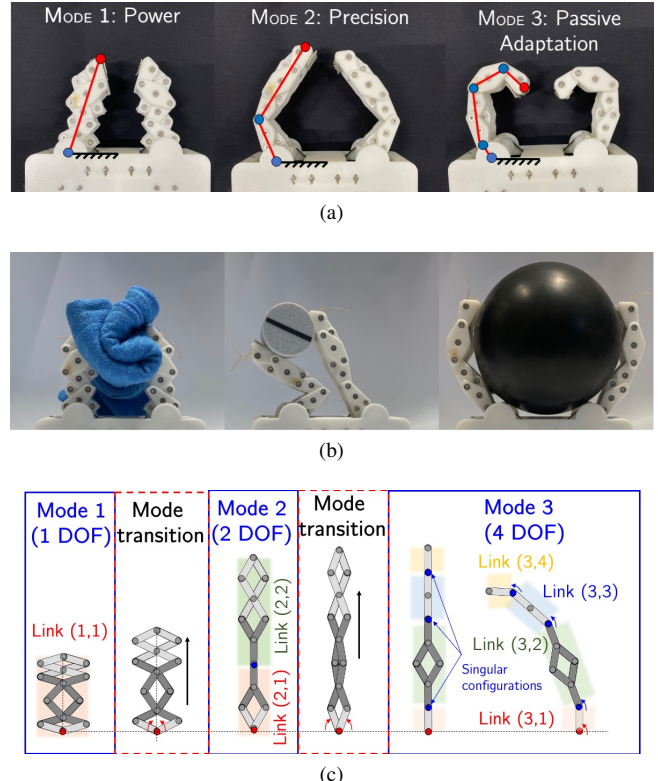


Fig. 1. Overview of the *multi-mode gripper*. (a) Actuating the finger linkage mechanisms switches between three kinematic modes, which are suited to tasks that require (respectively) maintaining a secure hold on an object or applying high pressure, precise finger positioning or in-hand manipulation, and passive adaptation to the shape of larger, delicate, or irregularly shaped objects. (b) Examples of such objects and tasks; see also Video 1. (c) A simplified model of a single finger, illustrating the linkage mechanism configurations in different modes and transitions between modes. In MODE 1, the links are fully retracted. During deployment, the base joint is driven by two motors that rotate towards each other. This causes the mechanism to extend to MODE 2 where the middle joint (blue) is in the singularity configuration. During the transition from MODE 2 to MODE 3, the base joint motors rotate again as to introduce singularities into three joints.

to handle. This task-specific design would be appropriate for industrial applications requiring repetitive grasping of a small number of distinct objects. However, a design specific to one task or object type may be insufficiently capable of handling other tasks or object types.

In this work, we focus on hardware innovations that increase grasp versatility in a single gripper. One approach to achieve robust grasping across a range of tasks and object types could involve switching between different modular end-effectors [3]. However, equipping multiple grippers may become a

disadvantage when storage space and total weight of a system are limited, and switching between end-effectors adds time to a grasping task. Another approach is a gripper that alters its kinematic and dynamic properties depending on the given task. For instance, finger stiffnesses can be modulated in pneumatic soft robots [4], [5], shape-memory polymer-based (SMP) robots, origami-based robots [6], [7], and microsurgical robots [8]. Other strategies include laminar jamming [9] and antagonistic tendons [10], [11], [12]. Still other grippers are designed with multiple grip modes that excel in handling small items [11], [12]. These hardware innovations can increase the range of object shapes, sizes, and textures that may be successfully managed by a single gripper. However, pneumatic actuators require bulky compressors and pumps; soft pneumatic actuators can leak and be punctured; and SMPs are energy inefficient [13]. Our design circumvents these issues via discrete mechanical transformations of scissor mechanisms composing the gripper's fingers, which enable strength, in-hand manipulation, and passive adaptation in three distinct modes.

Other work in multi-mode grippers has considered mechanically transforming grippers that, e.g., switch between parallel-jaw and adaptive gripping modes and adjust finger spacing to increase the area of the manipulation workspace [16], or assume a thinner configuration to access narrow spaces [17]. These examples switch between two modes, using more traditional mechanical designs and methods of transformation. Our design presented here transforms between three modes, using a scissor mechanism.

Robots utilizing scissor mechanisms offer compact storage and transport advantages. Such designs, like Teshigawara's scissor mechanism-based manipulator, yield expansive workspaces from compact configurations [18]. However, these are typically employed to extend reach, not to enhance end-effector grasping performance. Previous work has proposed deployable mechanisms with angulated elements, like Liu et al.'s shape-varied device using Bricard linkages [19]. Similarly, our device incorporates Bricard linkages and angulated scissor mechanisms, rooted in Hoberman's work [20], [21], to switch between three kinematic modes.

In this work, we present a multi-mode reconfigurable robotic gripper with switchable finger kinematics (Fig. 1). Multiple grip modes are implemented in a single gripper by using a scissor linkage design that has different locations and numbers of mechanical singularities as it extends and retracts, thereby switching its finger kinematics, actuation scheme, and geometry. MODE 1 effectively has a single linkage per finger, which is actuated by all three servos, and has a shorter length and a textured gripping surface; these features allow the finger to output higher forces and grip objects securely. MODE 2, with two independently controllable linkages, can excel in pinch grasping and in-hand manipulation, allowing more precise and dexterous grip (although decreasing grip force). MODE 3 has four degrees of freedom, three of which are controlled by a single cable-driven actuator. This underactuation allows the fingers to passively adapt to the shape of an object and distribute contact pressure (without complicated joint control), which is advantageous for grasping irregularly shaped, de-

formable, or delicate items. We discuss design, fabrication, and modeling considerations, and characterize the performance of the gripper experimentally. Kinematic modeling of the gripper enables controllers to be designed and verified in simulation. The model is sufficiently parametric such that a designer could design a custom gripper suited to their tasks.

## II. DESIGN AND FABRICATION

To demonstrate the benefits of our switchable kinematics in the gripper's fingers, we elected to utilize a two-finger gripper design, as opposed to adopting an anthropomorphic model. This design incorporates an angulated scissor linkage mechanism, characterized by joint singularities. As the scissor mechanism extends to MODE 2, the finger arrives at an initial singularity, effectively operating with a single internal joint. Subsequently, the finger reaches a second singular configuration, at which point it effectively functions with three internal joints in MODE 3. This unique design emphasizes our gripper's flexibility and adaptability.

Fig. 1c illustrates the mode transition process. In MODE 1, the finger is fully retracted. There is one rotational joint at the base to enable the gripping motion. To extend the scissor linkage and transform to MODE 2, the gears attached to the top and bottom servos rotate in opposite directions. In MODE 2, there is a singularity condition between the angulated elements. The result is an additional rotational joint at the middle of the linkage for a total of two degrees of freedom, i.e., two serially-connected links with two rotational joints. When the middle joint is rotated away from the straight configuration, other joints in the linkages are interlocked and the linkages can be considered as two rigid structures connected at the middle joint. To transform to the third mode, the middle joint is returned to the straight position and the linkage is then further extended. In MODE 3, the scissor mechanism is fully extended; three new singularity points appear, but one singularity point from MODE 2 vanishes. Rotation is permitted about the singularity points.

To drive each finger, two servo motors connect to the top and bottom of the base joint via a gear with a ratio of 1:1, and one bi-directional wire-based actuator drives the rotational joints within the finger (Fig. 2c). This wire mechanism enables the actuation scheme to change between fully-actuated (MODE 1 and MODE 2) and under-actuated (MODE 3) when the kinematic configuration is changed. The kinematic and dynamic differences between the three modes are:

- **MODE 1:** The Bricard-based finger is fully retracted and the grip motion has one degree of freedom. All three actuators (Fig. 2b) apply a rotating torque to the base joint while all scissor joints are interlocked such that the links behave as one rigid structure. In MODE 1, there is a mechanical advantage relative to MODE 2 and MODE 3 because the linkage is shorter, maximizing the fingertip force.
- **MODE 2:** In this mode, the base joint is actuated by all three actuators, but the middle joint is actuated by the cable servo. In this way, the two rotational joints can be independently controlled and various finger postures for dexterous grip can be achieved.

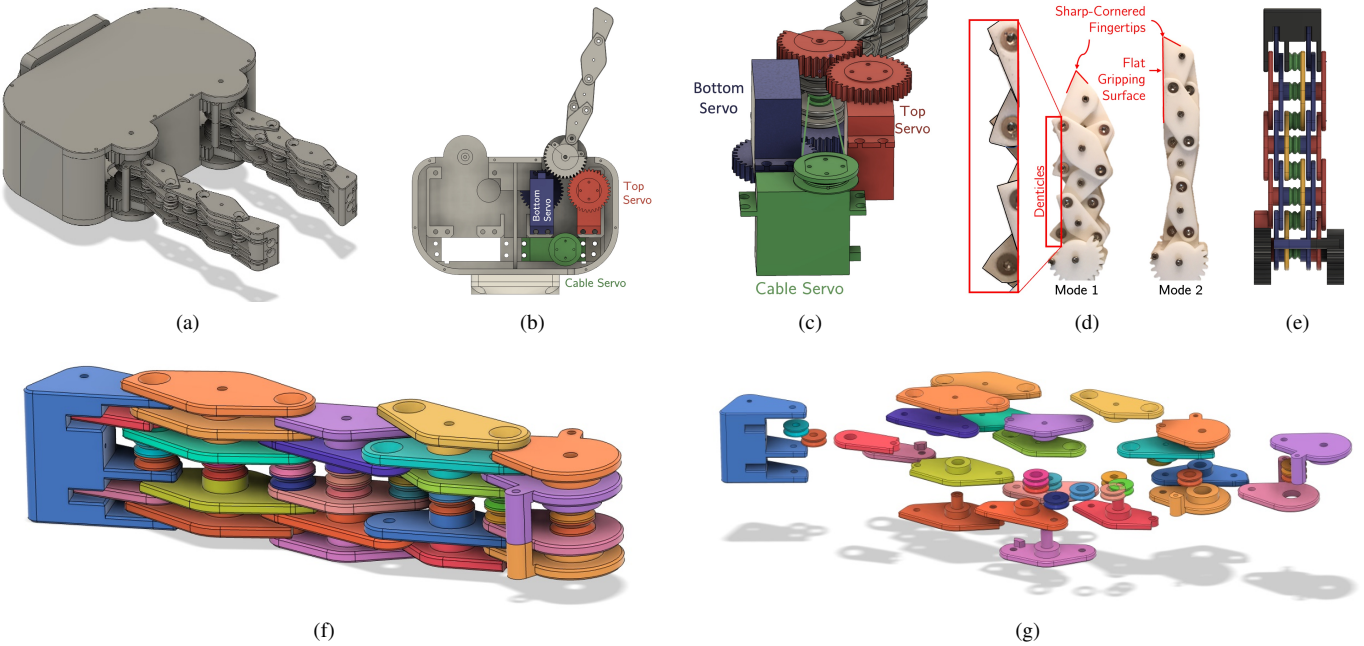


Fig. 2. Gripper design. (a) Rendering of the complete gripper. (b) Rendering with the servo box cover taken off. (c) Two servo motors connect to the top and bottom of the base joint via a gear with a ratio of 1:1, and one bi-directional wire-based actuator drives the rotational joints within the fingers. (d) In MODE 1, the sharp corners of the links reveal sharp denticles. These are inspired by the denticles in coconut crab (*Birgus latro*) claws [14], [15], and help maintain a secure grip. In MODE 2, the link geometry provides a flat gripping surface that is advantageous for in-hand manipulation. (e) The multiple layers in each finger of the gripper. The layer redundancy is indicated with blue and red (only one blue and red layer each are required; extra layers increase contact surface area and off-axis stiffness). (f) The assembled finger, shown here in MODE 3. The colors have no meaning except to distinguish separate components. (g) The “exploded” view of components.

- MODE 3: In this mode, the base joint is again actuated by all three actuators. The other three joints are actuated by the single cable servo, which makes these three joints underactuated and allows the fingers to passively adapt to an object shape without precise control.

Along with the kinematics and actuation mechanism, the shape and size of the gripper are also important design factors. In our prototype gripper, the fingers are sized similar to a human hand in order to handle common “everyday” objects. In MODE 1, the finger design exposes denticles inspired by crab claws (Fig. 2d). These teeth-like shapes may improve pull-out force on large objects and help to hold soft objects like fabrics. The denticles may also help to concentrate pressure, which could be advantageous for squeezing or crushing objects. In MODE 2, the distal link has a flat surface, which is advantageous when choosing a precision grip (Fig. 2d). The fingers were also designed to have multiple layers of linkages to provide sufficient contact surface area and increase off-axis stiffness (Fig. 2e). Pulleys were placed in the middle of the linkage layers for the wire-driven mechanisms. Fig. 2f,g shows an exploded view of the many linkages that compose the finger.

The body and linkages of the prototype were fabricated from polylactic acid (PLA) filament using a 3D printer (Prusa i3 MK3S+, Prusa Research). Six servos were housed in the body (MG996R, Deegoo-FPV). The cables of the gripper were stainless steel strand wires coated with nylon (JW12T-10FT, Beadalon). The mass of the gripper was 925 g and its thickness was 80 mm. The low-level servo control of

TABLE I  
PARAMETER VALUES FOR THE GRIPPER PROTOTYPE

Parameter	Value		
	Mode 1	Mode 2	Mode 3
$d_S$ (mm)		21	
$d_P$ (mm)		7	
$y_0$ (mm)		42.5	
$\tau_M$ (N·m)		0.92	
$L_{i1}$ (mm)	85.30	41.93	16.15
$L_{i2}$ (mm)	-	80.99	52.84
$L_{i3}$ (mm)	-	-	32.95
$L_{i4}$ (mm)	-	-	24.72
$F_{i1}/\tau_M (\frac{N}{N \cdot m})$	$2.79 \times 10^{-2}$	$5.68 \times 10^{-2}$	0.147
$F_{i2}/\tau_M (\frac{N}{N \cdot m})$	-	$4.70 \times 10^{-3}$	-

the gripper was realized using a microcontroller (Arduino Nano Every). Higher-level control including kinematics, mode changes, motion planning, the GUI, and coordination with a UR5e robotic arm was realized using ROS (Robot Operating System).

### III. KINEMATICS

The kinematics of the finger are modeled by first analyzing the transformation between the configuration space (joint angles) and task space (fingertip positions). Then, the actuation angles (servo rotation angles) are mapped to the configuration space. A diagram of the tendon routing and linkage lengths is provided in Fig. 3.

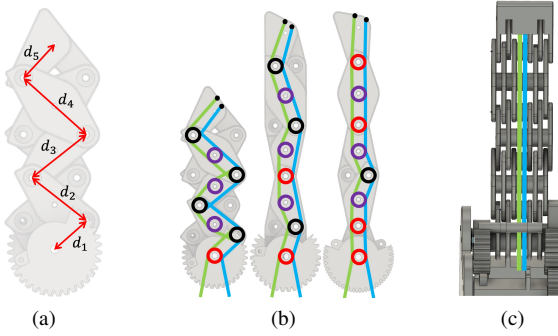


Fig. 3. (a) The link lengths,  $d_i$ , although depicted in MODE 1, are independent of the mode. (b) The routing of the tendons (blue=top, green=bottom) through the fingers in each mode. The singularities that create rotational joints are indicated with red circles. Black circles indicate bearings (pulleys) around which the tendons wrap one loop. The purple circles indicate bearings that the tendons go over but do not wrap. (c) The tendon locations as viewed from the inside side of the fingers.

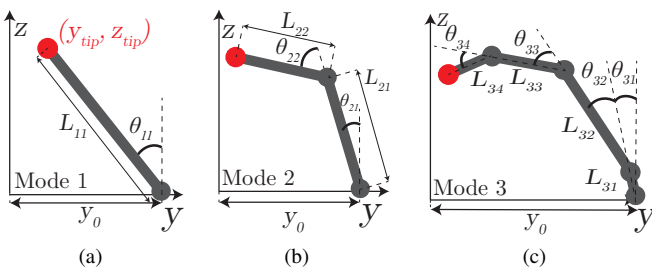


Fig. 4. For each mode, a schematic depicting the lengths  $L_{ik}$ , and joint angles  $\theta_{ik}$ , where  $i$  is the mode index and  $k$  is the link index. MODE 1 is shown in (a), MODE 2 in (b), and MODE 3 in (c).

### A. MODE 1

A kinematic diagram is provided in Fig. 4a. To go from joint space to task space, the forward kinematics for the position of the finger tip may be modeled as:

$$y_{\text{tip}} = y_0 - L_{11} \sin \theta_{11}, \quad z_{\text{tip}} = L_{11} \cos \theta_{11}, \quad (1)$$

where  $y_{\text{tip}}$  and  $z_{\text{tip}}$  are respectively the horizontal and vertical coordinates of the tip.  $L_{11}$  is the length of the first (and only) link in MODE 1.  $\theta_{11}$  is the orientation of Link 1, i.e., the rotation angle of the finger's proximal joint. We can rearrange Eq. (1) to obtain the inverse kinematics of MODE 1:

$$\theta_{11} = \sin^{-1} \left( \frac{y_{\text{tip}} - y_0}{-L_{11}} \right) \quad (2)$$

Given the mechanical design of the gripper, we can map the actuator space to the joint space as follows:

$$\phi_B = \theta_{11}, \quad \phi_T = \theta_{11}, \quad \phi_C = R\theta_{11}, \quad (3)$$

where  $\phi_B$ ,  $\phi_T$ , and  $\phi_C$  are the rotation angles of the base servo, top servo, and cable servo, respectively. Note that the base joint interacts with the top and bottom motors via gears of equal diameter, leading to a gear ratio of 1. The cable servo, however, possesses a spool of diameter  $d_S$  that interacts with the pulley of diameter  $d_P$ . Let us define the gear ratio,  $R$ , as

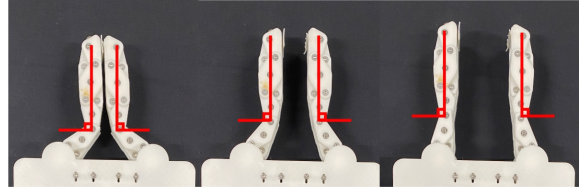


Fig. 5. Parallel grip in MODE 2.

$R = d_P/d_S$ . We assume no slipping between the cables and the pulleys. If  $d_P < d_S$ ,  $R < 1$  and the torque delivered by the cable servo is reduced.

### B. MODE 2

A kinematic diagram is provided in Fig. 4b. The forward kinematics that map  $[\theta_{21} \quad \theta_{22}] \rightarrow [y_{\text{tip}} \quad z_{\text{tip}}]$  are as follows:

$$\begin{aligned} y_{\text{tip}} &= y_0 - L_{21} \sin \theta_{21} - L_{22} \sin(\theta_{21} + \theta_{22}) \\ z_{\text{tip}} &= L_{21} \cos \theta_{21} + L_{22} \cos(\theta_{21} + \theta_{22}) \end{aligned} \quad (4)$$

We can firstly solve for  $\theta_2$  as follows:

$$\theta_2 = \cos^{-1} \left( \frac{(y_0 - y_{\text{tip}})^2 + z_{\text{tip}}^2 - L_{21}^2 - L_{22}^2}{2L_{21}L_{22}} \right). \quad (5)$$

We may then solve for  $\theta_1$ :

$$\theta_1 = \tan^{-1} \left( \frac{L_{22} \sin \theta_2 + L_{22} \cos \theta_2}{L_{21}} \right). \quad (6)$$

The rotation of each actuator is then:

$$\phi_B = \theta_1 + \psi_{12}, \quad \phi_T = \theta_1 - \psi_{12}, \quad \phi_C = \theta_1 + \psi_{12} + \theta_2 \quad (7)$$

where  $\psi_{12}$  is the rotation that enables the transition from MODE 1 to MODE 2.

A special case of MODE 2's operation is the parallel grip, as shown in Fig. 5. In this case, the servos change the width between the gripper's distal links while keeping them parallel to each other. To keep  $L_{22}$  parallel to the gripper's base frame, we can hold the rotation angle of the cable servo constant. Mathematically, this implies that  $\theta_{22} = -\theta_{21}$ . The forward kinematics to predict the tip position are:

$$y_{\text{tip}} = y_0 - L_{21} \sin \theta_{21}, \quad z_{\text{tip}} = L_{21} \cos \theta_{21} + L_{22} \quad (8)$$

If  $y_{\text{tip}}$  is given, the inverse kinematics can be computed as follows. Firstly,  $\sin \theta_{21} = \frac{y_0 - y_{\text{tip}}}{L_{21}}$ . The joint angles are then

$$\theta_{21} = -\theta_{22} = \sin^{-1} \left( \frac{y_0 - y_{\text{tip}}}{L_{21}} \right) \quad (9)$$

The actuator rotation is then:

$$\phi_B = \theta_1 + \psi_{12}, \quad \phi_T = \theta_1 - \psi_{12}, \quad \phi_C = \psi_{12} \quad (10)$$

Note that  $\psi_{12}$  is "leftover" from the mode transition from MODE 1 to MODE 2. That is, in the parallel grip mode, the cable servo does not move.

### C. MODE 3

The forward kinematics in MODE 3 are as follows, with the diagram provided in Fig. 4c:

$$\begin{aligned} y_{\text{tip}} = & y_0 - L_{31} \sin \theta_{31} \\ & - L_{32} \sin (\theta_{31} + \theta_{32}) \\ & - L_{33} \sin (\theta_{31} + \theta_{32} + \theta_{33}) \\ & - L_{34} \sin (\theta_{31} + \theta_{32} + \theta_{33} + \theta_{34}) \end{aligned} \quad (11)$$

$$\begin{aligned} z_{\text{tip}} = & L_{31} \cos \theta_{31} + L_{32} \cos (\theta_{31} + \theta_{32}) \\ & + L_{33} \cos (\theta_{31} + \theta_{32} + \theta_{33}) \\ & + L_{34} \cos (\theta_{31} + \theta_{32} + \theta_{33} + \theta_{34}) \end{aligned} \quad (12)$$

The rotation of each actuator is computed as follows:

$$\begin{aligned} \phi_B = & \theta_{31} + \psi_{23}, \quad \phi_T = \theta_{31} - \psi_{23}, \\ \phi_C = & \theta_{31} + \psi_{23} + \theta_{32} + \theta_{33} + \theta_{34} \end{aligned} \quad (13)$$

The system is under-actuated in MODE 3, with only the single input  $\phi_C$  available for control of the three degrees of freedom  $\theta_{32}, \theta_{33}, \theta_{34}$ . The inverse kinematics of MODE 3 are therefore redundant and undefined until the finger is in contact with an object.

## IV. STATIC FORCE ANALYSIS

In this section, we study the mapping from the motor torques to joint torques to fingertip forces.

### A. Torques at the Joints

To analyze the torques delivered to the joints in each mode, we use the principle of virtual work. This analysis also depends on gear ratios, the diameters to compute which are given in Table I.

1) MODE 1: In MODE 1, using the principle of virtual work, we balance the energies at the base joint:

$$\tau_B \delta(\phi_B) + \tau_T \delta(\phi_T) + \tau_C \delta(\phi_C) = \tau_{11} \delta(\phi_1), \quad (14)$$

where  $\delta(\cdot)$  is a function representing an infinitesimally small change in the attached angular value. Given that in MODE 1,  $\phi_B = \phi_T = (d_S/d_P)\phi_C = \theta_{11}$ , we can find the torque at joint 1,  $\tau_{11}$ :

$$\begin{aligned} \tau_B \delta(\theta_{11}) + \tau_T \delta(\theta_{11}) + \tau_C (R) \delta(\theta_{11}) = & \tau_{11} \delta(\theta_{11}) \\ \tau_{11} = & \tau_B + \tau_T + R \tau_C \end{aligned} \quad (15)$$

Therefore, the torque delivered to the base joint (Joint 1) is the sum of the torque delivered by each motor after accounting for the gear reduction due to the cable servo. This strengthens the grip force during MODE 1.

2) MODE 2: For MODE 2, we conduct a similar analysis, except that the finger now has two movable joints:

$$\tau_B \delta(\phi_B) + \tau_T \delta(\phi_T) + \tau_C \delta(\phi_C) = \tau_{21} \delta(\theta_{21}) + \tau_{22} \delta(\theta_{22}) \quad (16)$$

Based on the kinematics of MODE 2, we can rewrite the energy balance as:

$$\begin{aligned} \tau_B \delta(\theta_{21}) + \tau_T \delta(\theta_{21}) + R \tau_C \delta(\theta_{21} + \theta_{22}) = & \\ \tau_{21} \delta(\theta_{21}) + \tau_{22} \delta(\theta_{22}) \end{aligned} \quad (17)$$

Notice that the cable servo delivers torque to both Joints 1 and 2. If we are interested in the maximum applicable torque at Joint 1, we may command the cable servo to not move Joint 2 (setting  $\phi_C = \theta_{21} + \psi_{21}$ ). In that case, similar to MODE 1, the maximum torque deliverable to Joint 1 is given in Eq. (15). If we hold the base joint fixed (by setting  $\phi_B = \psi_{12}$ ,  $\phi_T = \psi_{12}$ , and  $\phi_C = \theta_{22} + \psi_{12}$ ), then the maximum torque  $\tau_2$  delivered to Joint 2 is:

$$\tau_{22} = \frac{d_P}{d_C} \tau_C. \quad (18)$$

3) MODE 3: In MODE 3, the analysis is similar to MODE 2, but the torques at each joint become indeterminate without knowledge of the externally applied forces resulting from a grasped object.

$$\begin{aligned} \tau_B \delta(\phi_B) + \tau_T \delta(\phi_T) + \tau_C \delta(\phi_C) = & \\ \tau_{31} \delta(\theta_{31}) + \tau_{32} \delta(\theta_{32}) + \tau_{33} \delta(\theta_{33}) + \tau_{34} \delta(\theta_{34}) \end{aligned} \quad (19)$$

We may substitute Eq. (13) into Eq. (19) to obtain

$$\begin{aligned} \tau_B \delta(\theta_{31}) + \tau_T \delta(\theta_{31}) + \tau_C \delta(\theta_{31} + \theta_{32} + \theta_{33} + \theta_{34}) = & \\ \tau_{31} \delta(\theta_{31}) + \tau_{32} \delta(\theta_{32}) + \tau_{33} \delta(\theta_{33}) + \tau_{34} \delta(\theta_{34}) \end{aligned} \quad (20)$$

If we only move Joint 1, then  $\tau_{31} = \tau_C + \tau_B + \tau_T$ . However, if we move Joints 2–4, then

$$\tau_C = \tau_{32} + \tau_{33} + \tau_{34} \quad (21)$$

This shows that the cable servo alone delivers torque to Joints 2–4, but we can not analytically determine the torque on an individual joint.

### B. Forces at the Fingertips

The maximum forces deliverable to the fingertips depend on (1) the specific mode, (2) the joint torques  $\tau_{ij}$ , and (3) the lever arm lengths  $L_{ij}$ . For this analysis, we consider the case where a force is applied perpendicular to the end of each link in each mode. The case for MODE 2 is depicted as an example in Fig. 6. A shorter lever arm is advantageous. To generalize the understanding of this system, we express fingertip force normalized to the motor torque. We assume that each servo in the gripper is identical and thus can deliver an equivalent amount of torque. That is, we assume  $\tau_M = \tau_B = \tau_T = \tau_C$ , where  $\tau_M$  is the maximum torque that each servo can continuously output within its safe operating range. For our prototype,  $\tau_M$  is provided in Table I. Note that this model assumes negligible joint friction; the prototype used lubricated bearings that helped reduce friction at the joints.

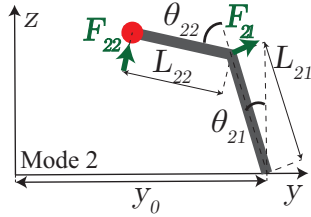


Fig. 6. A model of the forces applied to the gripper, shown here in MODE 2 as an example.

1) MODE 1: In MODE 1, the fingertip force normalized to the motor torque is:

$$F_{11}/\tau_M = (2+R)/L_{11} \quad (22)$$

2) MODE 2: When only Link 1 is moving, we may assume that all three motors contribute to the motion of the first link, as in MODE 1:

$$F_{21}/\tau_M = (2+R)/(L_{12}) \quad (23)$$

However, the second link may only receive torque from the cable servo:

$$F_{22}/\tau_M = R/L_{22} \quad (24)$$

Despite the relative low force output of the second link, the advantages of MODE 2 are its ability to position the fingertips at arbitrary points in the workspace, achieve a parallel grasp configuration, and perform in-hand manipulation.

3) MODE 3: Given that MODE 3 is under-actuated, the force modeling becomes ambiguous in the three most distal links of the gripper. The force output of the first link is computed in the same manner:

$$F_{31}/\tau_M = (2+R)/L_{31} \quad (25)$$

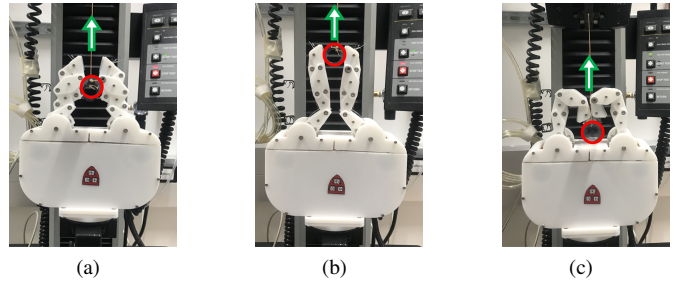
Note that because Link 1 of MODE 3 is quite short (16.15 mm), the force output is relatively high compared to the other modes. Specific values for the force-to-torque ratios are provided in Table I.

## V. EXPERIMENTAL DEMONSTRATIONS

### A. Pullout Force

To compare the relative grip strength of different modes, the pullout force was measured (Fig. 7a–c). The base of the gripper was fixed to the lower end of a single-column Instron testing machine, a small (10-mm diameter) or medium (30-mm diameter) rigid cylinder was suspended from the upper end, and the gripper’s fingers were closed around the object with the maximum torque permitted by its motors (0.92 N·m for our prototype). The upper end of the Instron was moved upward until the cylinder exited the gripper’s grasp, and the maximum force up until that point was recorded. The cylinders were acrylic plastic with 5 mm wall thickness.

Fig. 7d shows the pullout force for both cylinders and all three modes. As expected, the pullout force is greatest in MODE 1, and lowest in MODE 2. Note that the low pullout



(a) (b) (c)

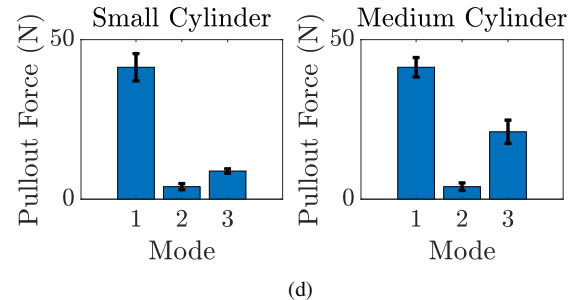


Fig. 7. The experimental setup for the pullout force in (a) MODE 1, (b) MODE 2, and (c) MODE 3. The test object is an acrylic cylinder and highlighted in red. (d) The experimental results. For each mode and test object, results are averaged over five trials, with the error bars showing standard deviation.

force for MODE 2 is affected both by grip strength being limited by the strength of the cable servo alone, and by the configuration of the fingers: an attempt to squeeze while using a parallel grip results in the second joints bowing inward, reducing pullout force compared to a caging grasp.

### B. Fingertip Force

To measure the fingertip force, one finger was held against a six-axis load cell (RFT60-HA01, Robotous), as shown in Fig. 8a. Then, the maximum torque permitted by the motor is applied to the joints by creating forced position error and generating corresponding torque from the servo’s internal controller. The measured force in MODES 1, 2, and 3 was  $16.6 \pm 0.3$  N,  $2.67 \pm 0.01$  N, and  $1.93 \pm 0.02$  N, respectively (standard error of the mean over five trials in each mode). The calculated fingertip force for MODES 1 and 2 is 21.9 N (Eqn. 22) and 3.29 N (Eqn. 24), respectively, with no prediction for MODE 3 since that mode is under-actuated. The discrepancies between empirical and theoretical values for MODES 1 and 2 are likely due to joint friction, which the theoretical models did not account for. The greater force for MODE 1 allows the gripper in that mode to crush objects not possible for the other modes (Fig. 8b).

### C. Model Verification

We experimentally validated our kinematic analysis using MODE 2 (since MODE 1 has trivial kinematics and MODE 3 is under-actuated). The left finger was commanded to sweep out an arc (Fig. 9a), passing through 16 waypoints equally spaced between the initial position of  $[\theta_{21}, \theta_{22}] = [-55^\circ, 0]$  and the final position of  $[\theta_{21}, \theta_{22}] = [18^\circ, 0^\circ]$ . This trajectory was chosen as one that activated all three servos and spanned

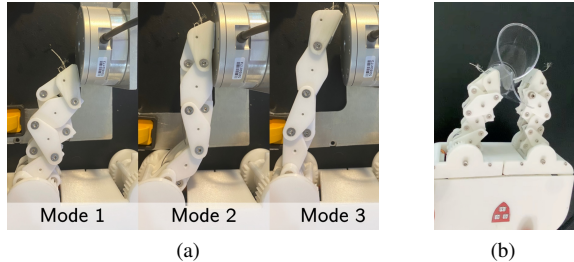


Fig. 8. (a) For each mode, the fingertip force was measured by pressing against a six-axis load cell. (b) The greater force available to MODE 1 allows it to perform tasks not possible for the other modes, e.g., crushing a cup.

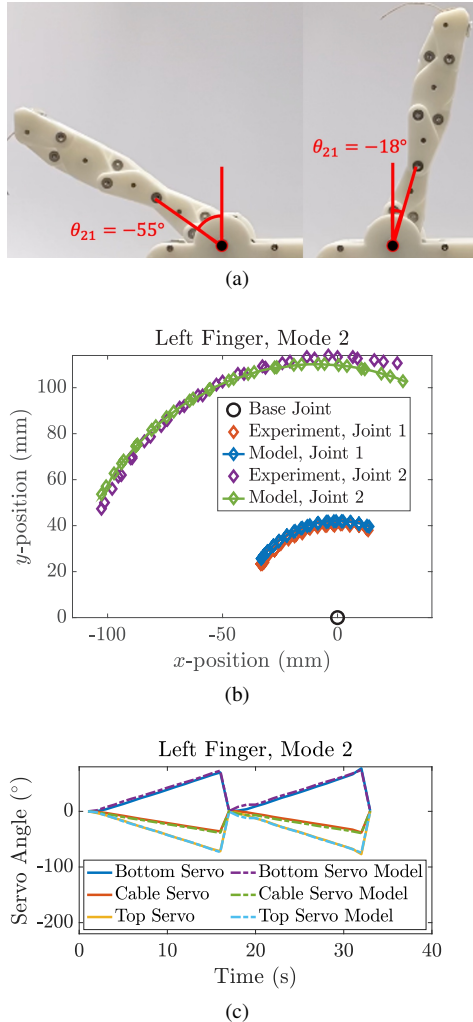


Fig. 9. A comparison of the model prediction versus the experimental results for MODE 2. (a) The initial and final position of the left finger during the experiment. (b) Depiction of Cartesian position of the predicted ( $x, y$ ) position and the modeled ( $x, y$ ) position. (c) The actual and modeled actuator input sequences. The modeled actuator inputs are determined based on the link angles observed during the experiments.

nearly the full workspace of the finger. Note that although the setpoint of  $\theta_{22}$  remained constant throughout the trajectory, achieving that constant angle requires all three servos to be active. Fig. 9b–c shows the calculated and empirical values for Cartesian joint coordinates and servo angles throughout the experiment. Summary statistics (mean and standard deviation) were computed based on  $N_s = 33$  samples, taken over two

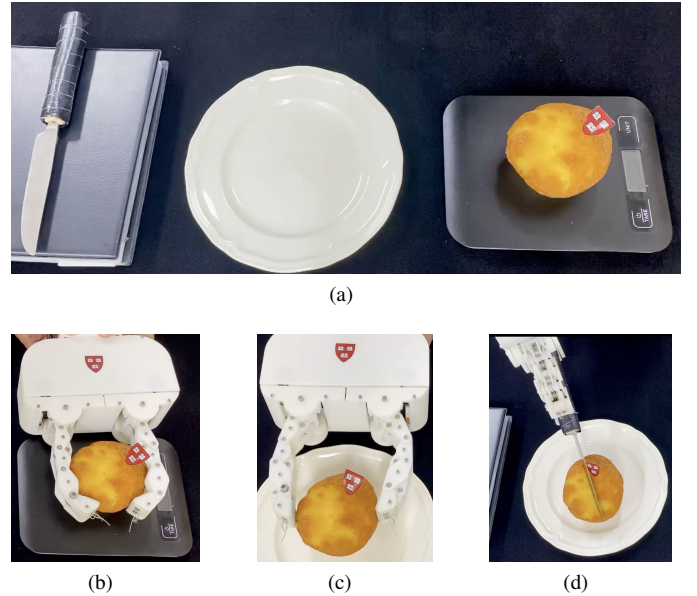


Fig. 10. Screenshots from Video 1 showing the gripper using three modes to conduct a complex multi-stage task. (a) Initial setup. (b) MODE 3 passively adapts to the shape of the muffin to transport it to the plate without damage. (c) MODE 2 rotates the muffin on the plate. (d) MODE 1 holds a knife to slice the muffin.

cycles of the full trajectory. The position error was  $1.6 \pm 0.6$  mm for Joint 1,  $5.6 \pm 0.9$  mm for Joint 2; the servo angle errors were  $3.20^\circ$ ,  $0.82^\circ$ , and  $2.24^\circ$  for the bottom, cable, and top servos, respectively.

#### D. Example Use Case

We demonstrate the multi-mode gripper's utility on an example food preparation task that requires different grasp properties at different stages (Fig. 10, Video 1). The task is to transport a muffin from a staging area, reorient it for presentation, and cut it with a knife. MODE 3 passively adapts gently to the shape of the muffin; MODE 2 allows the gripper to rotate the muffin in-hand; MODE 1 holds the knife securely for cutting.

Video 1 demonstrates also how inappropriate choice of mode at any stage can lead to task failure. In the first step, MODE 1 crushes the muffin. In the second step, MODE 3 requires motion of the whole gripper to reorient the muffin. In the third step, MODE 2 cannot hold the knife.

## VI. DISCUSSION AND CONCLUSION

In this study, we have introduced a multi-mode gripper with fingers featuring switchable kinematics, mechanically increasing its range of grasping capabilities. We derived kinematic models pertinent to the operational modes and validated their respective advantages via a hardware prototype.

This new gripper concept could be used for complex tasks necessitating varying degrees of strength, precision, and passive adaptation at different stages throughout the task (Fig. 10, Video 1). In addition to everyday domains like food preparation, another area where such capabilities could be valuable is space applications; Fig. 11 shows a prototype gripper mounted on NASA's Valkyrie robot [22]. Our work demonstrates the

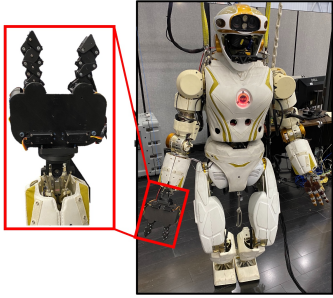


Fig. 11. A prototype of the multimode gripper mounted on Valkyrie, NASA’s first bipedal humanoid robot [22].

potential for a single end-effector that can adapt to dynamic task requirements, providing versatility needed for possible use in real-world applications.

The kinematic results, as shown in Fig. 9, affirm that our modeling strategy accurately describes the gripper’s kinematics. Nonetheless, we observed some deviation between the modeled outcomes and the actual experimental results. These discrepancies could originate from various sources. One plausible cause could be the varying tension in the cables throughout the experiment’s trajectory. Excessive tension could result in considerable resistance in the second linkage, while inadequate tension could lead to backlash between the rotation of the cable servo and the movement of the second linkage. These considerations indicate areas for improvement in both fabrication and modeling of the gripper.

The hardware prototype shows several limitations: (1) 3D printing using PLA may cause deviations in behavior; using instead a metal like aluminum could improve stiffness. (2) Lack of integration with a full manipulation stack hinders evaluation against other systems. (3) Weak motors limit force capabilities; higher-torque motors could improve this. (4) Encoders in finger joints would enhance precision. (5) Force sensors would help monitor gripper-object interactions.

In future work, we hope to develop a high-level controller that permits an autonomous robot to intelligently select between the three modes during dynamic operations. The inputs for this controller would predominantly be derived from the objectives of the task and the properties of the object involved (mass, volume, geometry, material stiffness, etc). The output would determine the best mode for a given situation, according to the detailed needs of the task at hand.

#### ACKNOWLEDGMENTS

The authors thank Dr. Daniel Bruder for feedback. The authors would also like to thank the members of the Dexterous Robotics Team at NASA Johnson Space Center for their collaboration.

#### REFERENCES

- [1] M. R. Cutkosky *et al.*, “On grasp choice, grasp models, and the design of hands for manufacturing tasks.” *IEEE Transactions on Robotics and Automation*, vol. 5, no. 3, pp. 269–279, 1989.
- [2] A. M. Okamura, N. Smaby, and M. R. Cutkosky, “An overview of dexterous manipulation,” in *Proceedings 2000 ICRA. Millennium Conference. IEEE International Conference on Robotics and Automation. Symposia Proceedings (Cat. No.00CH37065)*, vol. 1, 2000, pp. 255–262.
- [3] J. Li, C. Teeple, R. J. Wood, and D. J. Cappelleri, “Modular end-effector system for autonomous robotic maintenance & repair,” in *2022 International Conference on Robotics and Automation (ICRA)*, 2022, pp. 4510–4516.
- [4] C. B. Teeple, T. N. Koutros, M. A. Graule, and R. J. Wood, “Multi-segment soft robotic fingers enable robust precision grasping,” *The International Journal of Robotics Research*, vol. 39, no. 14, pp. 1647–1667, 2020.
- [5] S. Abondance, C. B. Teeple, and R. J. Wood, “A dexterous soft robotic hand for delicate in-hand manipulation,” *IEEE Robotics and Automation Letters*, vol. 5, no. 4, pp. 5502–5509, 2020.
- [6] A. Firouzeh and J. Paik, “Grasp mode and compliance control of an underactuated origami gripper using adjustable stiffness joints,” *IEEE/ASME Transactions on Mechatronics*, vol. 22, no. 5, pp. 2165–2173, 2017.
- [7] A. Firouzeh, M. Salerno, and J. Paik, “Stiffness control with shape memory polymer in underactuated robotic origamis,” *IEEE Transactions on Robotics*, vol. 33, no. 4, pp. 765–777, 2017.
- [8] J. Kim, W.-Y. Choi, S. Kang, C. Kim, and K.-J. Cho, “Continuously variable stiffness mechanism using nonuniform patterns on coaxial tubes for continuum microsurgical robot,” *IEEE Transactions on Robotics*, vol. 35, no. 6, pp. 1475–1487, 2019.
- [9] Y. S. Narang, J. J. Vlassak, and R. D. Howe, “Mechanically versatile soft machines through laminar jamming,” *Advanced Functional Materials*, vol. 28, no. 17, p. 1707136, 2018.
- [10] R. Konda, D. Bombara, S. Swanbeck, and J. Zhang, “Anthropomorphic twisted string-actuated soft robotic gripper with tendon-based stiffening,” *IEEE Transactions on Robotics*, 2022.
- [11] T. Nishimura, K. Mizushima, Y. Suzuki, T. Tsuji, and T. Watanabe, “Variable-grasping-mode underactuated soft gripper with environmental contact-based operation,” *IEEE Robotics and Automation Letters*, vol. 2, no. 2, pp. 1164–1171, 2017.
- [12] T. Watanabe, K. Morino, Y. Asama, S. Nishitani, and R. Toshima, “Variable-grasping-mode gripper with different finger structures for grasping small-sized items,” *IEEE Robotics and Automation Letters*, vol. 6, no. 3, pp. 5673–5680, 2021.
- [13] J. Zhang, J. Sheng, C. T. O’Neill, C. J. Walsh, R. J. Wood, J.-H. Ryu, J. P. Desai, and M. C. Yip, “Robotic artificial muscles: Current progress and future perspectives,” *IEEE Transactions on Robotics*, vol. 35, no. 3, pp. 761–781, 2019.
- [14] M. N. Rosen, K. A. Baran, J. N. Sison, B. V. Steffel, W. C. Long, R. J. Foy, K. E. Smith, R. B. Aronson, and G. H. Dickinson, “Mechanical resistance in decapod claw denticles: Contribution of structure and composition,” *Acta Biomaterialia*, vol. 110, pp. 196–207, 2020.
- [15] T. Inoue, S.-i. Oka, K. Nakazato, and T. Hara, “Columnar structure of claw denticles in the coconut crab, *Birgus latro*,” *Minerals*, vol. 12, no. 2, p. 274, 2022.
- [16] N. Elangovan, L. Gerez, G. Gao, and M. Liarokapis, “Improving robotic manipulation without sacrificing grasping efficiency: a multi-modal, adaptive gripper with reconfigurable finger bases,” *IEEE Access*, vol. 9, pp. 83 298–83 308, 2021.
- [17] T. Nishimura, T. Muryoe, Y. Asama, H. Ikeuchi, R. Toshima, and T. Watanabe, “Single-fingered reconfigurable robotic gripper with a folding mechanism for narrow working spaces,” *IEEE Robotics and Automation Letters*, vol. 7, no. 4, pp. 10 192–10 199, 2022.
- [18] S. Teshigawara and H. H. Asada, “A mobile extendable robot arm: singularity analysis and design,” in *2019 IEEE/RSJ International Conference on Intelligent Robots and Systems (IROS)*. IEEE, 2019, pp. 5131–5138.
- [19] R. Liu, R. Li, and Y.-A. Yao, “Reconfigurable deployable bricard-like mechanism with angulated elements,” *Mechanism and Machine Theory*, vol. 152, p. 103917, 2020.
- [20] Z. E. Teoh, B. T. Phillips, K. P. Becker, G. Whittredge, J. C. Weaver, C. Hoberman, D. F. Gruber, and R. J. Wood, “Rotary-actuated folding polyhedrons for midwater investigation of delicate marine organisms,” *Science Robotics*, vol. 3, no. 20, p. eaat5276, 2018.
- [21] C. Hoberman, “Radial expansion/retraction truss structures,” Jun. 18 1991, US Patent 5,024,031.
- [22] N. A. Radford, P. Strawser, K. Hambuchen, J. S. Mehling, W. K. Verdeyen, A. S. Donnan, J. Holley, J. Sanchez, V. Nguyen, L. Bridgewater *et al.*, “Valkyrie: Nasa’s first bipedal humanoid robot,” *Journal of Field Robotics*, vol. 32, no. 3, pp. 397–419, 2015.